Experimental Thermal and Fluid Science 75 (2016) 25–34

Contents lists available at ScienceDirect

Experimental Thermal and Fluid Science

journal homepage: www.elsevier.com/locate/etfs

Densification of frost on hydrophilic and hydrophobic substrates – Examining the effect of surface wettability

Andrew D. Sommers *, Nicholas L. Truster, Andrew C. Napora, Aaron C. Riechman, Edgar J. Caraballo

Department of Mechanical and Manufacturing Engineering, Miami University, 56 Garland Hall, 650 East High Street, Oxford, OH 45056, USA

ARTICLE INFO

Article history:
Received 20 August 2015
Received in revised form 7 November 2015
Accepted 12 January 2016
Available online 22 January 2016

Keywords:
Frost growth
Aluminum
Contact angle
Surface wettability
Density
Frost thickness
Hydrophilic
Hydrophobic

ABSTRACT

The properties of a growing frost layer were analyzed and compared for surfaces of different wettability to determine the effect that the surface energy has on the frost mass, thickness, and density. Three surfaces were tested – an uncoated, untreated aluminum plate (Surface 1), an identical plate coated with a hydrophobic coating (Surface 2), and a plate containing a hydrophilic coating (Surface 3). For these experiments, the frost layer was grown for a three-hour period inside a Plexiglas environmental test chamber where the relative humidity was held constant (i.e. 60%, 80%) using an ultrasonic humidifier. The surface temperature of the plate was fixed using a thermoelectric cooler (TEC) and monitored by four thermocouples affixed to the surface and stage. Frost thickness was determined from images of the frost layer taken using a CCD camera mounted directly overhead. A reduction in frost density of 37–41% was observed on the hydrophobic surface (Surface 2), whereas an increase of 20–26% was consistently observed on the hydrophilic surface (Surface 3) as compared to the baseline surface. Frost layer property data were also compared against models found in the literature. Reasonably good agreement was observed when comparing against data from the baseline surface; however, the agreement was not generally as good when compared against the hydrophilic and hydrophobic surfaces suggesting the need for surface wettability to be included as a parameter in future frost densification models.

1. Introduction

The study and continued development of super-hydrophilic and super-hydrophobic surfaces represents a valuable step in advancing our current understanding and design of more energy efficient and frost tolerant systems. For example, in refrigeration systems, heat exchanger fin spacing is often quite large to mitigate frost blockage of the air flow passage, and thus the convective heat transfer coefficient is typically low. Because of the requirement for periodic defrosting, refrigerator evaporators tend to be rather inefficient due to this periodic downtime. Furthermore, because the frost layer acts as an additional thermal resistance, the cooling capacity of the evaporator tends to decrease with ongoing frost layer growth. Thus, the development of more accurate frost growth and densification models represents an important issue for the HVAC&R industry; however, it is also expected that this research would benefit the aerospace and automotive industries where these models might be used to help mitigate surface drag, improve wing de-icing, etc. It is also important to note that while methods currently exist for creating water repellent and/or frost tolerant surfaces, these approaches typically rely upon chemical coatings which break down over time due to the thermal cycling and large temperature gradients experienced in these systems.

Over the years, numerous frost studies and frost densification models have been published. For example, O'Neal and Tree [1] and Padki et al. [2] have each performed an extensive review of the literature and tried to summarize the effect that various environmental parameters have on frost properties. Östin and Andersson [3] concluded that the plate surface temperature and the air relative humidity both affect frost thickness; whereas, the density of the frost largely depends on the air velocity and to a lesser extent on the relative humidity. Density, however, was independent of surface temperature. Similarly, the mass deposition rate of the frost was shown to have considerable dependence upon the relative humidity and air velocity. Östin and Andersson [3] also examined the contribution of the mass flux of condensed vapor to frost density and frost thickness and found that the condensing water vapor contributes nearly equally to the increase of frost density and frost thickness. Rite and Crawford [4] examined the impact that various environmental parameters have on the frost rate of an evaporator and found that a theoretical frost deposition rate based on measured upstream and downstream relative humidities was reasonably accurate. They also observed that the average frosting

* Corresponding author.
E-mail address: sommerad@miamioh.edu (A.D. Sommers).

http://dx.doi.org/10.1016/j.expthermflusci.2016.01.008
0894-1777/

Nomenclature

A	heat transfer area (mm^2)
c_p	specific heat of air ($J\,kg^{-1}\,K^{-1}$)
CA	contact angle (°)
F_t	function defined by Eq. (5) (–)
i_{sv}	latent heat of sublimation ($J\,kg^{-1}$)
k	thermal conductivity ($W\,m^{-1}\,K^{-1}$)
m	frost mass (g)
p	vapor pressure (Pa)
RH	relative humidity (%)
t	time (sec)
T	temperature (°C)
V	voltage (V)

Greek Symbols

δ	frost thickness (mm)
Λ	modified Jakob number
Π	ratio defined by Eq. (4)
ρ	density ($kg\,m^{-3}$)
ω	humidity ratio ($kg_v\,kg^{-1}$)

Subscripts

a	air
f	frost
m	melting point
sat	saturation
w	plate surface

rate flux was essentially the same after 10 h as it was after 5 h, whereas Senshu et al. [5] had suggested that the frosting rate decreased with increasing air velocity. Other relevant works include Hayashi et al. [6] who derived a correlation to calculate the frost density, and Brian et al. [7] who developed a correlation for calculating the effective thermal conductivity of the frost layer based on the mean frost surface temperature and the average frost density. Other published methods for predicting frost properties on conventional surfaces (esp. thermal conductivity) include Yang and Lee, Yang et al., Yonko and Sepsy, and Lee et al. [8–11].

Using the frost property models of Hayashi et al. [6] and Brian et al. [7], Cheng and Cheng [12] proposed a theoretical model for predicting the frost growth rate on a flat plate. Assumptions inherent to this model included uniform frost density throughout the frost layer at any instant, orthogonal growth of the frost layer relative to the plate surface, uniform frost thickness, and constant heat and mass transfer coefficients (h and h_m) on the frost surface. Comparisons were made with other existing theoretical models by Jones and Parker [13] and Sherif et al. [14]. Cheng and Wu [15] examined frost formation on a flat plate subjected to atmospheric air flow in an open-loop wind tunnel using a CCD camera. They distinguished between three different time periods in the formation of frost as was done previously by Hayashi et al. [6] and called them the *crystal growth period*, *frost layer growth period*, and *full growth period*, respectively. More recent models for the prediction of the frost growth rate use supersaturated water vapor at the frost surface instead of saturated vapor such as Na and Webb [16,17]. Other relevant models of frost growth and densification include Cheng and Cheng [12], Cheng and Wu [15], Schneider [18], Tao et al. [19], White and Cremers [20], Yun et al. [21], Inaba and Imai [22], Le Gall and Grillot [23], and Ogawa et al. [24].

One of the best recent works that was found on frost layer densification is by Hermes et al. [25]. In this work, the authors presented a first-principles based model for predicting the time-evolving porosity of a frost layer. This theoretical model was then combined with experimental data (obtained elsewhere) to produce a semi-empirical correlation for frost layer densification as a function of time and the modified Jakob number. It is also worth noting that most correlations for frost density in the literature rely upon the frost surface temperature such as Hayashi et al. [6] which is difficult to obtain. The model by Hermes et al. [25] was independent of the frost surface temperature while still providing an explicit relationship between frost density and time. In a follow-up work by the same group, Nascimento et al. [26] extended this work to create a model for frost build-up between two parallel plates in channel flow.

With regards to predicting frost layer thickness, several researchers have suggested that the increase in frost thickness is nearly proportional to the square root of time during the mature growth period including Östin and Andersson [3], Schneider [18], Hoke et al. [27], and Okoroafor and Newborough [28]. In the work by Schneider [18], frost thickness was found to be largely independent of certain parameters that are often important in mass transfer such as the Reynolds number and the vapor pressure difference between the air stream and the frost surface. Instead, the frost thickness followed crystal growth behavior which is affected by the ratio of supersaturation and the conduction of the heat of sublimation that is delivered when the water molecule is built into the lattice. An equation based on a simplified model of frost growth was derived and compared against measured experimental data. The equation was found to be in good agreement with the data with a probable error of ±3.7% and a maximum error of ±10%. In the work by Okoroafor and Newborough [28], crosslinked hydrophilic polymeric coatings were examined as a possible means of retarding frost growth as compared to an uncoated aluminum surface. In this study, tests were performed at two plate temperatures (i.e. −5 °C and −10 °C) and two relative humidities (i.e. 40% and 70%), and then a regression analysis was performed to determine the constants that best fit their experimental data. The extent of the reduction in frost growth appeared to vary with the water absorbing potential of the polymeric coating.

Although many studies have been performed to model frost properties, relatively few papers were found which specifically examined the effect of surface wettability on the growing frost layer. In fact, in most published work on frost properties, the effect of the substrate surface energy has been largely ignored which may explain some of the scatter that has been reported in the literature. Some papers, however, have examined the impact of surface wettability on frost growth [29–31]. In a paper by Shin et al. [29], three different surfaces having advancing dynamic contact angles (DCA) of 23°, 55°, and 88° were installed in a wind tunnel and exposed to a humid air flow. They found that during the initial period of frost formation, the shape of the micro droplets depended upon the surface energy, and the process of frost growth was affected by the advancing DCA. High DCA surfaces showed the presence of irregular and rough crystals during the initial period of frost deposition, which resulted in high frost thickness and low frost density. By comparison, low DCA surfaces showed uniform and regular crystals resulting in low frost thickness and high density. This suggests that the growth of crystals is strictly controlled by surface energy during the early stages of frost growth. However, when the frost thickness was observed to reach a certain level, frost formation tended to be influenced instead by the environmental conditions rather than by the surface characteristics. One of the main limitations of this paper (and their associated model) is that this work

Table 1
Matrix of heat transfer test surfaces.

No.	Material	Surface features	Method
1	Al	None	–
2	Al	Hydrophobic coating (NeverWet™ spray-on coating)	Spray coating
3	Al	Hydrophilic silane (3:2 amino silane/sulfur silane)	Immersion

only considered surfaces of varying hydrophilicity (not hydrophobicity) and only one surface temperature (−22 °C) was examined which is significantly lower than the present study. Likewise, only hydrophilic coatings were examined in the paper by Okoroafor and Newborough [28]. Hoke et al. [27] examined surfaces that were both hydrophilic and hydrophobic; however, the advancing contact angle on the hydrophobic surface was only 106° with an accompanying receding contact angle of 84°. In a more recent study, Kulinich et al. [30] showed that super-hydrophobic surfaces are not always ice-repellent and that the ice-repellent properties of super-hydrophobic materials can deteriorate during icing/deicing cycles due to damage to the surface asperities. They also showed that the anti-icing efficiency of super-hydrophobic surfaces is significantly lower in a humid atmosphere due to increased ice adhesion strength. In summary, very few papers exist in the open literature in which surface wettability is specifically included in the published frost layer densification model. For those that do exist, the range of applicability is still quite limited (i.e. only hydrophilic substrates, one surface temperature, etc.). This highlights the need for improved models to be developed and for additional research to be performed in this area.

2. Experimental methodology

2.1. Experimental test conditions and surfaces

In this study, the frost experiments performed were primarily concerned with studying the properties of the growing frost layer. During these tests, the surface temperature was prescribed using a thermoelectric cooler (TEC). The air temperature and relative humidity were also recorded during each test and held constant using cool mist humidification. Experiments were three hours in duration followed by ten minutes of defrosting. The test samples were constructed from aluminum alloy 5052 polished on one side to a brushed finish. The plates were affixed to the TEC stage using thermal paste and four Nylon screws with Teflon spacers to minimize water retention and thermal losses from the surface. The test surfaces all had the same dimensions and were approximately 99.5 mm × 80.2 mm × 3.4 mm in size. The total surface area of the plates was 7979.9 mm^2. Details about the various plates and their differences in wettability can be found below in Table 1. One plate contained a commercially available hydrophobic coating (i.e. NeverWet), and the other was prepared with a hydrophilic silane coating which consisted of an amino silane (i.e. $C_8H_{22}N_2O_3Si$) and a sulfur silane (i.e. $C_{18}H_{42}O_6S_4Si_2$) in a 3:2 M ratio. The silane was first dissolved in a 95% ethanol/water mix. The surface was then immersed in the silane solution for approximately 5–10 min and cured at 100 °C for 30 min. Table 2 shows the various operating conditions associated with each experiment.

Table 2
Matrix of experimental test conditions.

RH (%)	Temp		
	−4 to −5 °C[a] (16.0 V TEC)	−7 to −8 °C[a] (18.6 V TEC)	−10 to −11 °C[a] (22.0 V TEC)
60	X	X	X
80	X	X	X

[a] Typical range.

2.2. Environmental test chamber

All experiments were performed in an environmental test chamber. To isolate the environmental conditions, a Plexiglas enclosure with a hinged, sealable lid was placed around the equipment as shown in Fig. 1. This Plexiglas enclosure had the dimensions 400.1 mm × 257.2 mm × 285.8 mm. A Plexiglas partition was inserted vertically inside the box to create a front and rear chamber inside of the enclosure, thereby permitting higher relative humidities to be achieved near the sample and to help maintain a constant air temperature inside the front chamber. This partition was secured so as not to affect the balance. An ultrasonic cool mist humidifier was used to maintain the relative humidity inside the test chamber to within ±2.5% of the desired value, and the air temperature inside the enclosure was typically held constant to within ±0.5 °C as shown in Figs. 2 and 3. An OMEGA OM-73 temperature/relative humidity data logger was used to record the environmental conditions during each test (±2% RH accuracy).

A GP5202 Sartorius balance connected to a laptop through a small hole in the rear partition of the Plexiglas enclosure was used for the real-time measurement of the frost mass. The frost mass was sampled and recorded at a frequency of approximately once every 0.2 s. A CP-061 Peltier thermoelectric cold plate cooler placed atop the balance and connected to a DC power supply was used to cool the surface. To accurately measure the frost growth, frost was only permitted to grow on the face of the test plate. To ensure frost growth only occurred on the test plate, multiple layers of insulation tape were placed around the edges of the thermoelectric cooler (TEC). A drip guard (isolated from the rest of the equipment) was placed underneath the face of the thermoelectric cooler to prevent any condensate and/or melted frost from draining onto the balance and affecting the mass measurement. The test plate was secured to the face of the thermoelectric cooler with Nylon screws and spacers to prevent frost build-up on the head of the screws. Thermal paste was used to secure the test plate to the face of the thermoelectric cooler and to help minimize the contact resistance between the plate and the stage. Four T-type thermocouples were used to measure the plate and stage temperatures (two on each side) during an experiment. The stage temperature was determined using two thermocouples affixed directly to the TEC surface by epoxy. The test plate temperature was determined using two thermocouples inserted into small holes drilled into the side of the test plates (one on each side). The depth of the holes was approx. 6–8 mm. Thermal paste was applied to the thermocouple junction before insertion, and epoxy was used to hold the thermocouple securely in place.

At the start of each test, the desired voltage was set for the TEC, and a thin plastic sheet was applied to the test surface to prevent condensation and/or frosting on the surface before the desired surface temperature was reached. Once the set-point temperature was reached, the plastic sheet was removed and the frost growth period was started. All tests were performed at constant voltage to the TEC. Defrosting was initiated by turning 'OFF' the power to the TEC and allowing the stage to warm up to room temperature and melt the frost. A Pixelink PL-B871CU CCD camera (1392 × 1040 resolution; 10 fps) placed on top of the Plexiglas enclosure (parallel to the face of the test plate) was used to record pictures of the frost thickness every 5 min during the frost growth period and every 30 s during defrosting. At the start of every experiment, a calibration image was taken. Pixel counting techniques were then used to determine the thickness of the frost layer as a

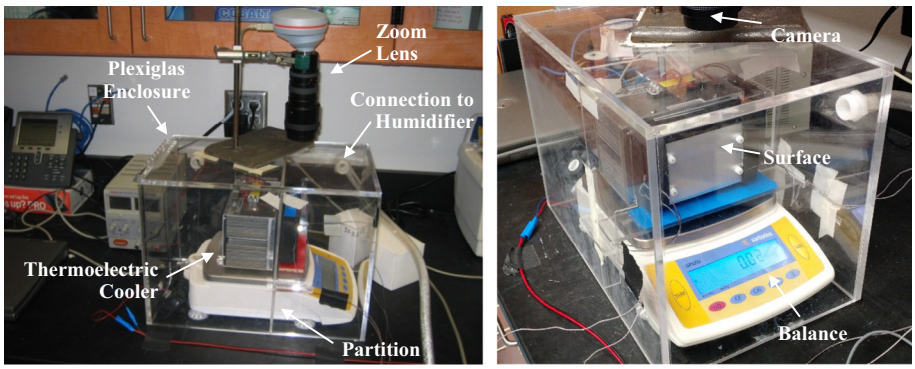

Fig. 1. Picture of experimental setup.

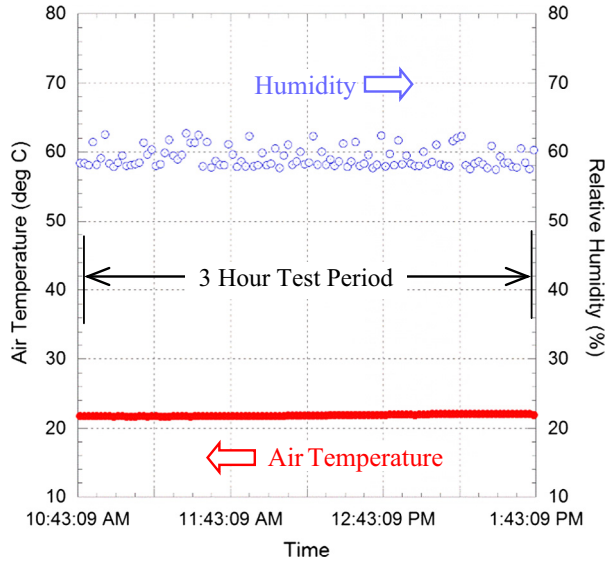

Fig. 2. Relative humidity and air temperature during a typical test with Surface 3 (60% RH, 22.0 V TEC).

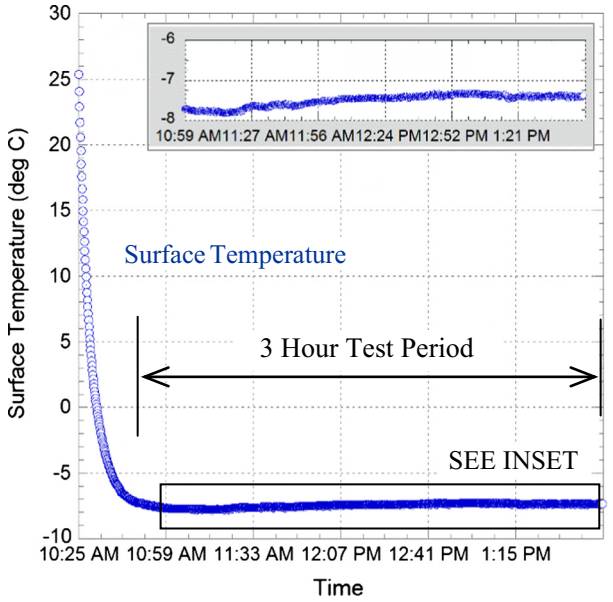

Fig. 3. Average plate temperature during a typical test with Surface 3 (60% RH, 18.6 V TEC).

Table 3
Summary of experimentally measured variables.

	T_{air}	T_w	RH	δ	m_f	ρ_f	θ
Measured	X	X	X	X	X		X
Calculated						X	

function of time. Depending on the level of the magnification, the resolution of the frost images varied from 0.015 to 0.024 mm/pixel. When coupled with the mass measurement, the average density of the frost layer could also be determined experimentally as a function of time (see Table 3).

3. Results and discussion

3.1. Contact angle data

Surface energy is most commonly quantified by measuring the contact angle that a droplet makes with a surface. Hydrophilicity (i.e. higher surface energy) is indicated by smaller contact angles, and hydrophobicity (i.e. lower surface energy) is indicated by high contact angles. In this work, a ramé-hart contact angle goniometer was used to measure the static, advancing and receding contact angles formed by water droplets injected on the test samples using the sessile drop method (see Table 4). As shown in this table, Surface 2 possessed a static contact angle of more than 150° which classifies the surface as being "super-hydrophobic." This contact angle was more than 50° higher than the baseline surface (i.e. Surface 1). It is also important to note that while there was an apparent decrease in the static contact angle following testing, the surface largely retained its hydrophobicity during these short-duration repeated experiments. Since that time, however, the surface has shown some evidence of losing its hydrophobicity

Table 4
Static, advancing, and receding contact angles on test plates.

	Surface description	θ_{static} (°)	θ_{adv} (°)	θ_{rec} (°)
1	Baseline surface (after cleaning)[a]	81.9	99.4	50.2
	Baseline surface (after testing)	98.1	101.1	54.5
2	Hydrophobic surface (not used in testing)[a]	158.9	162.2	154.8
	Hydrophobic surface (after testing)	151.5	–	–
3	Hydrophilic surface (not used in testing)[a]	45.3	64.7	18.1

[a] An additional surface was used for these measurements.

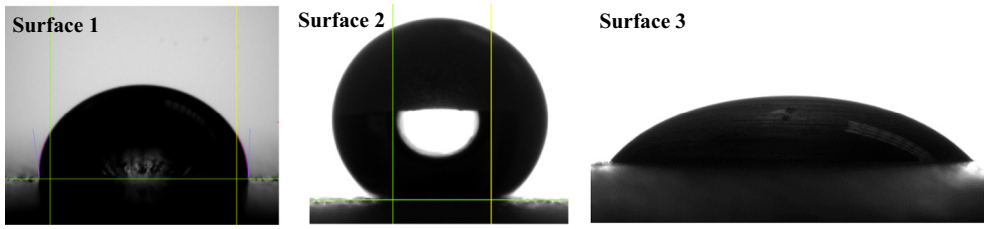

Fig. 4. Static contact angles on the three surfaces.

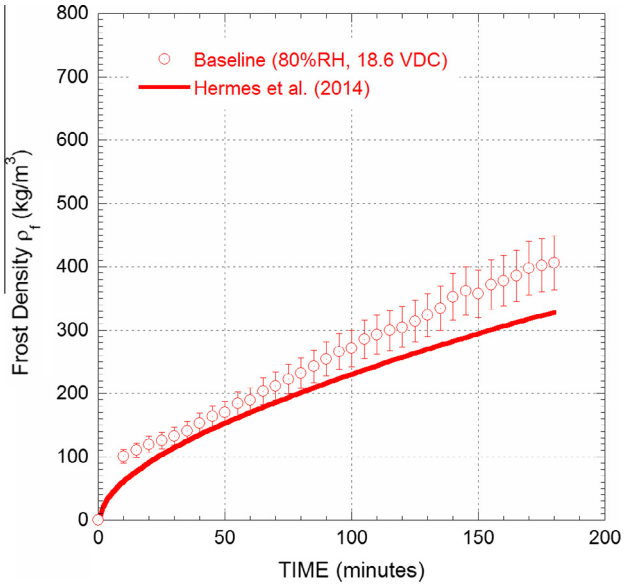

Fig. 5. Benchmarking of experimental data with the Hermes et al. [25] model.

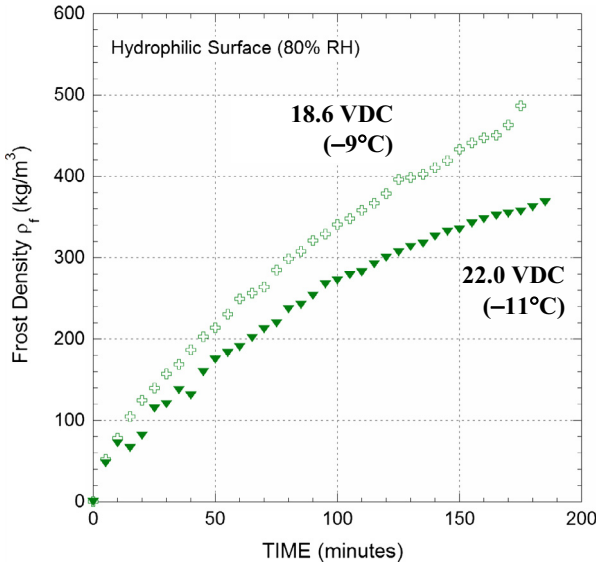

Fig. 7. Frost density on Surface 3 for two different surface temperatures at fixed 80% RH.

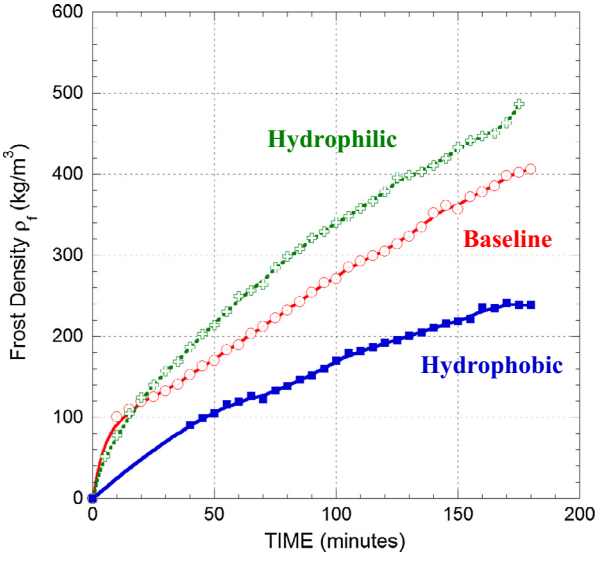

Fig. 6. Frost density comparison between the surfaces for 80% RH and 18.6 VDC.

which is consistent with the findings of other researchers who have reported that super-hydrophobic materials can deteriorate in ice-repellency following multiple icing/deicing cycles [30]. In contrast, the static contact angle on Surface 3 was 45.3°. Also noteworthy, the contact angle hysteresis (i.e. $\theta_{adv} - \theta_{rec}$) of Surface 3 was more than 46°, while the hysteresis of Surface 2 was less than 8°. (Note: Small contact angle hysteresis values are often associated with increased droplet mobility and therefore reduced water retention.) In all cases, more than 25 measurements were recorded using the goniometer at different locations on the surface in arriving at these average values. The uncertainties associated with the baseline surface measurements were ±3.3°, ±1.4°, and ±2.3° for the static, advancing, and receding contact angles, respectively. Fig. 4 shows representative images of water droplets on the various test surfaces (i.e. Surfaces 1–3). As will be shown later, surface energy (i.e. wettability) can have a significant effect on the properties of a growing frost layer as well as water removal efficiency during a defrosting event.

3.2. Frost density data

Initially, our calculated frost density data were checked against published models found in the literature in order to validate and check our overall experimental approach. As stated earlier, one of the best recent works on frost layer densification is by Hermes et al. [25], and thus it was chosen for benchmarking purposes. In this work, a first-principles based approach was used for predicting the time-evolving porosity of a frost layer. A semi-empirical correlation for frost layer densification is then given as a function of time and the modified Jakob number as shown below:

$$\rho_f = 2.2\Lambda^{-3/2}\sqrt{t} \tag{1}$$

where the modified Jakob number is defined as

$$\Lambda = \frac{c_p}{i_{sv}} \frac{T_{sat,a} - T_w}{\omega_a - \omega_{sat,w}} \tag{2}$$

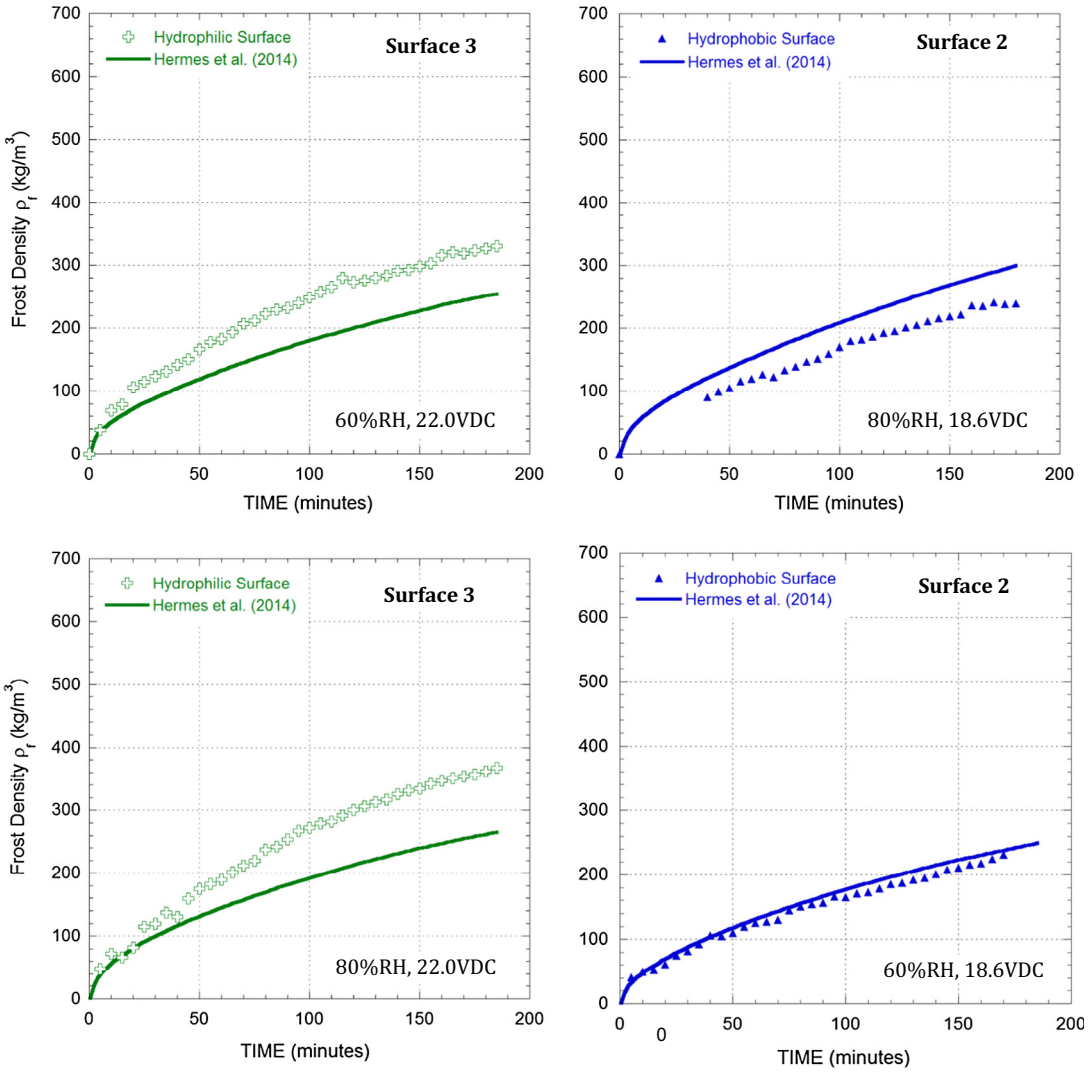

Fig. 8. Frost density comparison with the Hermes et al. [25] correlation on both the hydrophilic sample (Surface 3) and the hydrophobic sample (Surface 2).

It should be noted that this correlation does not require the frost surface temperature to be known as do some other correlations. It only requires the plate temperature to be known (T_w). In this way, it represents a more convenient and more easily implementable equation for predicting the density of a frost layer. Shown in Fig. 5 is a comparison between the frost density data for one of our baseline surface experiments and this published model. The average error between the model and the data was 16.4%. Overall, reasonably good agreement was observed with the best agreement occurring during early densification of the frost layer when the experimental uncertainty was smallest.

Next, the experimental frost density was examined on both the hydrophobic and hydrophilic plates (i.e. Surfaces 2 and 3). As can be seen in Fig. 6 for fixed operating conditions (80% RH, 18.6 VDC), the frost density was highest on the hydrophilic plate (Surface 3) and lowest on the hydrophobic plate (Surface 2). More specifically, beyond the initial 30 min of frosting, the density on Surface 3 was observed to be consistently 20–26% higher than the frost density on the baseline surface. This result is consistent with the findings of Shin et al. [29] and Lee et al. [31] who both reported denser frost formation on surfaces with lower dynamic contact angles (DCA). In contrast, the frost density on Surface 2 (hydrophobic) was consistently 37–41% lower than the frost density on the baseline surface as shown in Fig. 6. These trends were observed multiple times and for different operating conditions. Overall, these results are consistent with other researchers who have suggested that surface wettability can affect mature frost growth properties through its effect on condensate distribution during the early stages of frost formation [27]. For example, it has been hypothesized that the formation of large discrete droplets on hydrophobic (low surface energy) substrates during the condensation period may lead to a fluffier, thicker frost layer; whereas the formation of a condensate film on a hydrophilic (high surface energy) substrate may lead to a thinner, denser frost layer. These results certainly support this idea.

In Fig. 7, the frost density is plotted for Surface 3 (hydrophilic) at fixed relative humidity (i.e. 80% RH) and two different plate temperatures (i.e. −9 and −11 °C). As shown here, the frost density is observed to be higher on the warmer surface (i.e. −9 °C) versus the colder surface (i.e. −11 °C). The increase in density was on average 24–28% higher. This result was also observed on the other two surfaces and is consistent with the findings of other researchers such as Hayashi et al. [6] and Östin and Andersson [3] who both found that low surface temperatures result in a frost layer of lower density.

In Fig. 8, frost density data are plotted for Surface 2 and 3 and compared against the Hermes et al. [25] correlation, which is one of the best frost layer densification models currently available in the literature. In this figure, it can be seen that the Hermes et al. [25] correlation overpredicts the experimental frost density on the hydrophobic surface (Surface 2) and underpredicts the frost density

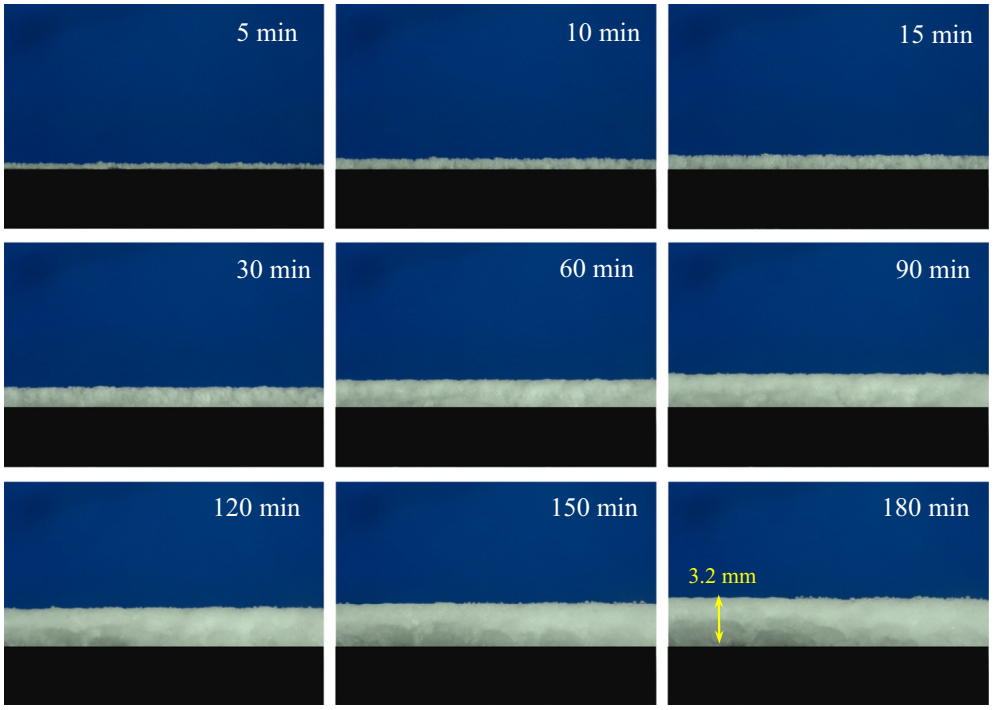

Fig. 9. Images of the growth of the frost layer on Surface 3 taken using an automated capture system for 60% RH, 16.0 VDC.

Table 5
Frost thickness parameters for uncoated Al from [28].

	T_w (°C)	RH (%)	b_1	n
Test 1	−10	70	0.22	0.54
Test 2	−5	70	0.19	0.55
Test 3	−10	40	0.07	0.75
Test 4	−5	40	0.08	0.66

on the hydrophilic surface (Surface 3). More specifically, the Hermes et al. [25] correlation overpredicts the frost density on the hydrophobic surface in this case by an average of 25.6% (n = 29) and 6.9% (n = 32); while it underpredicts the frost density on the hydrophilic surface by an average of 26.0% (n = 36) and 25.3% (n = 35). Similar levels of agreement were observed for the other operating conditions; however, qualitative agreement with the correlation tended to be worse on the hydrophilic surface (Surface 3) in terms of its transient behavior. In fact, in all test cases, the correlation underpredicted the frost density on the hydrophilic surface by an average of at least 17%. In a couple of cases, the underprediction of the frost density on Surface 3 was as high as 36–43%. Overall though, the level of agreement tended to be worse on the hydrophilic surface (Surface 3) than the hydrophobic surface (Surface 2). Interestingly, but perhaps not surprisingly, the amount of deviation for the two surfaces was of similar proportion to the level of increase (or decrease) that was observed in the static contact angle for these two surfaces relative to the baseline surface. These results point to the need for surface wettability to be included in future frost densification models. Currently, the authors are aware of only one published paper in the open literature in which surface wettability (or, contact angle) is included explicitly in the model [29], and this paper only examined hydrophilic surfaces at a considerably lower cold plate temperature (i.e. −22 °C). If surface wettability is known to affect the mode of condensation (i.e. dropwise vs. filmwise) on the surface as well as the initial distribution of water on the surface during the early frost growth period [27], one might expect that the properties of the frost layer during the mature growth period would still be impacted.

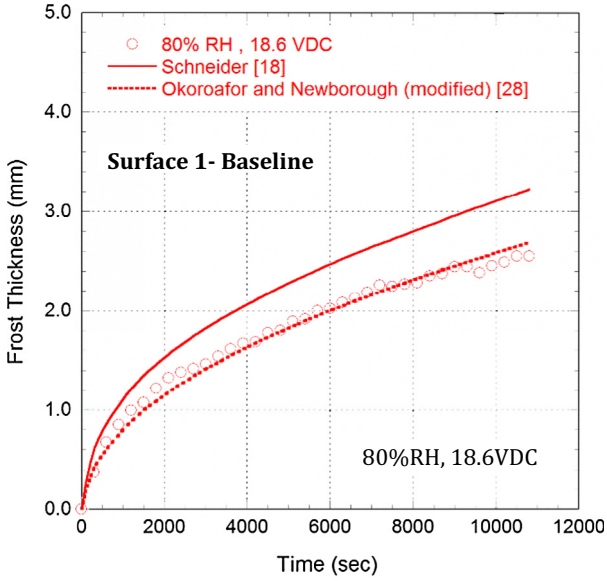

Fig. 10. Comparison of frost thickness on Surface 1 (baseline) versus theoretical models [18,28].

3.3. Frost thickness data

Next, the transient behavior of the frost layer thickness on both the baseline surface and the two test surfaces was examined as a function of the operating conditions. An automated image capture system was used to take high-quality images of the frost layer at a fixed time interval of every five minutes, and the frost thickness was then measured locally at three different locations along the surface and averaged. Fig. 9 shows images of the frost layer on Surface 3 at different time intervals. (Note: The surface is in a vertical orientation.) The frost thickness was then compared against two published models for frost growth. It is important to point

out that both of these models exclude contact angle as a parameter. In Schneider [18], frost growth is modeled assuming crystals growing from the gaseous phase where

$$\delta = 0.465\left[\frac{k_{ice}\cdot t}{\rho_{ice}\cdot i_{sv}}\cdot(T_f - T_w)\right]^{1/2}\left(\frac{t}{3600}\right)^{-0.03}(T_f - T_w)^{-0.01}\prod^{0.25}F_t \quad (3)$$

where

$$\prod = \frac{p_v - p'_{sat,f}}{p'_{sat} - p'_{sat,f}} \quad (4)$$

$$F_t = 1 + 0.052\frac{T_a - T_m}{T_m - T_w} \quad (5)$$

and T_m represents the melting point temperature of water–ice, T_a is the air temperature, T_w is the plate temperature, p_v is the partial vapor pressure of the air, p'_{sat} is the vapor pressure of saturated air, and $p'_{sat,f}$ is the vapor pressure of saturated air at the frost surface temperature. In Okoroafor and Newborough [28], the following frost growth model is proposed

$$\delta = b_0 + b_1\cdot t^n \quad (6)$$

where the parameters b_1 and n were specified by the authors for different experimental conditions (see Table 5). The relative humidity of the air was shown to have a stronger influence on these two parameters than the plate temperature. Based on these reported values and taking the frost thickness to be zero at $t = 0$, the following models were assumed

$$\delta = 0.12\cdot t^{0.58} \text{ for } 60\%\text{ RH} \quad (7a)$$

$$\delta = 0.20\cdot t^{0.50} \text{ for } 80\%\text{ RH} \quad (7b)$$

(Note: These models were not reported in [28]. Instead, they were assumed based on the parameters given in [28] for an uncoated aluminum surface at similar plate temperatures and relative humidities as those used in this work.)

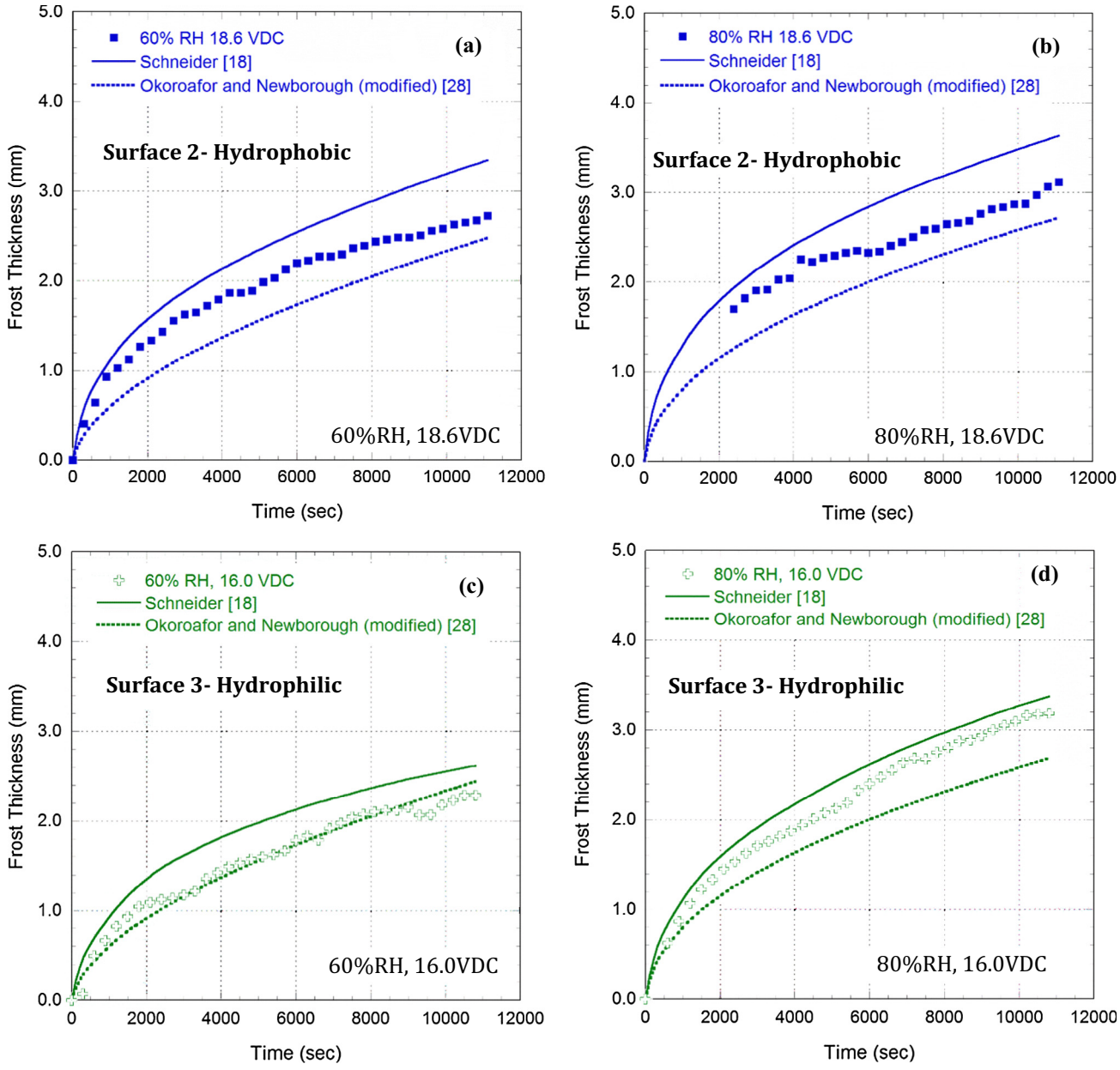

Fig. 11. Comparison of frost thickness on Surfaces 2–3 versus theoretical models [18,28].

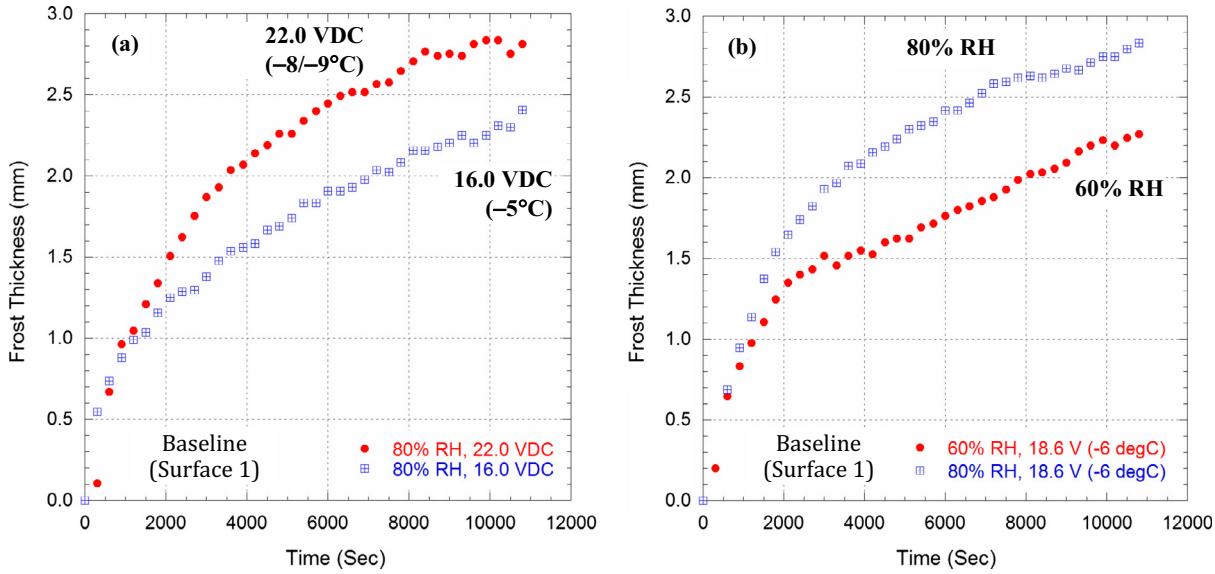

Fig. 12. Effect of surface temperature and relative humidity on frost thickness for the baseline surface.

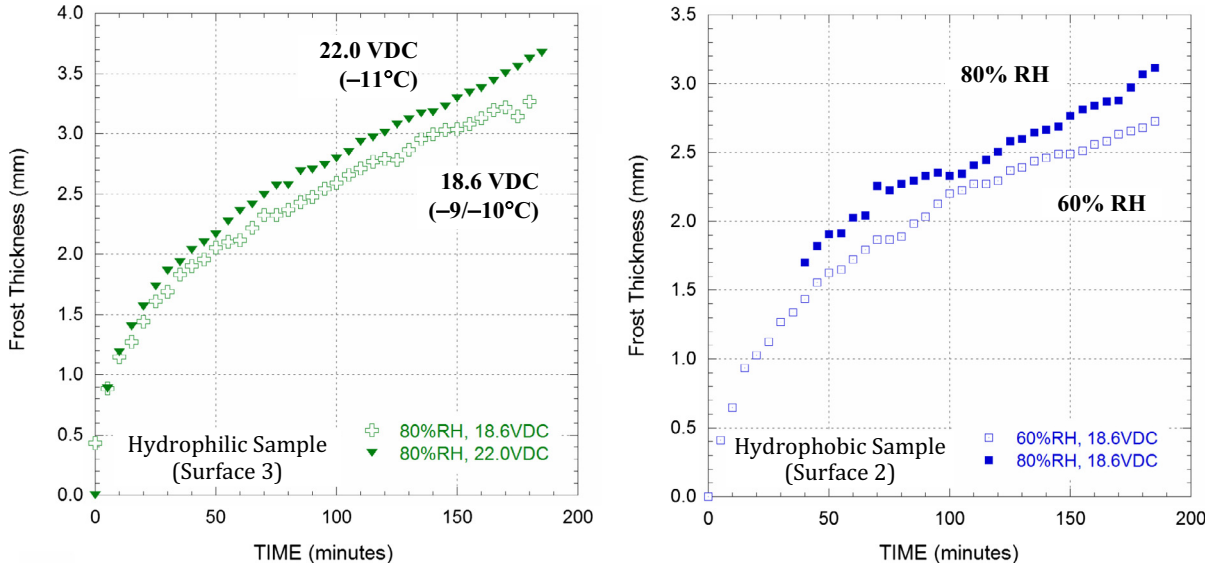

Fig. 13. Effect of surface temperature and relative humidity for Surfaces 2 and 3.

In Figs. 10 and 11, experimental frost thickness data for Surfaces 1–3 are compared against both of these models, namely – Schneider [18] and the modified Okoroafor and Newborough [28] correlations. As shown in these figures, both of the models do reasonably well at predicting the frost thickness under different operating conditions on all three surfaces. In general, however, slightly better agreement was observed using the modified Okoroafor and Newborough [28] correlation (i.e. Eqs. (7a) and (7b)). The best agreement was observed on the baseline surface (Surface 1) and hydrophilic surface (Surface 3). For example, the average error between the baseline data shown in Fig. 10 and the modified Okoroafor and Newborough [28] correlation was 4.2% after the first five minutes of frost growth. If the first 30 min of frost growth is excluded, the error drops to 3.2%, and if the first hour of frost growth is excluded, the error is only 2.3%. In contrast, the level of agreement was not as good on the hydrophobic sample (Surface 2). The average error between the hydrophobic data shown in Fig. 11a and the predicted value using Eq. (7a) is 20.5% when all data are considered for $t > 0$ and 16.4% if the first hour of frost growth is excluded. This decrease in prediction accuracy was observed on Surface 2 for other operating conditions as well (see Fig. 11b). The reason for this is presently unclear but may be related to differences in frost growth behavior on hydrophilic and hydrophobic surfaces during the condensation and early frost growth periods. On hydrophobic surfaces, condensate droplets are more raised up on the surface. On baseline and hydrophilic surfaces, condensate droplets are generally flatter.

In Fig. 12, the frost thickness on the baseline surface (Surface 1) is shown first as a function of the surface temperature (holding RH constant) and then as a function of the air relative humidity (holding surface temperature constant). As seen in the figure, the frost thickness is observed to scale inversely with the surface temperature (see Fig. 12a) but directly with the relative humidity (see Fig. 12b). Thus, the frost thickness was greatest on the −9 °C surface (versus the −5 °C surface) and on the surface exposed to 80% RH (versus 60% RH). This was predicted by Hayashi et al. [6]

who found that thinner, denser frost layers formed on warmer surfaces and thicker frost layers were formed on colder surfaces. In another work [11], the influence of relative humidity was examined, and the frost layer thickness was shown to increase with humidity. In both cases, the differences in frost thickness on Surface 1 were not apparent until after approximately 1500 s of frosting. The maximum observed difference in frost thickness was approx. 0.5–0.6 mm.

The effect of surface temperature and relative humidity on frost thickness on the hydrophilic and hydrophobic samples (i.e. Surfaces 2 and 3) is shown in Fig. 13. As can be seen in this figure, the same behavior was observed on these surfaces as was observed on the baseline surface. Higher specific humidity values tend to produce thicker frost layers overall due to the higher mass transfer rate, and colder plate temperatures tend to produce thicker frost layers due to differences in the type of frost crystals that are formed on the surface. The uncertainty in the frost thickness varied from ±0.02–0.15 mm with the largest uncertainties typically occurring near the end of the experiment. During the first 120 min of frost growth, the uncertainty was usually less than ±0.05 mm.

4. Conclusions

In this work the properties of a growing frost layer for surfaces of varying wettability were analyzed to determine the effect that the surface energy has on the frost thickness and density. The experimental methodology was validated using a baseline surface (Surface 1) by comparing the measured frost density against a published correlation found in the literature by Hermes et al. [25]. These results for the frost density as a function of time showed good overall agreement with the frost density predicted using this semi-empirical method derived from first-principles. Frost thickness data were also checked against published models from the literature [18,28] with good agreement generally being observed.

The effect of surface energy on the frost thickness and density was then investigated for both a hydrophobic substrate (Surface 2) and a hydrophilic substrate (Surface 3). The frost layer on the hydrophobic surface was "thicker and fluffier" resulting in a less dense frost than the frost on the baseline surface. Reductions in frost density of 37–41% were observed on Surface 2. Conversely, the density of the frost layer on the hydrophilic surface (Surface 3) was consistently 20–26% higher than the frost density on the baseline surface. This increase in density which likely stems from the initial distribution of water on the surface could provide an operational benefit since the conduction of heat through a denser frost layer is expected to be higher due to increased thermal conductivity of the frost. Moreover, these results suggest that surface energy does affect the properties of a growing frost layer beyond the initial condensation period suggesting that surface wettability modification could be used to enhance system performance in refrigeration applications.

It should also be noted that frost density correlations found in the open literature generally do not include surface wettability (i.e. contact angle) as a parameter in the model. Our research, however, has shown that surface wettability is important in accurately determining the properties of the frost layer and thus should be included in future frost correlation development efforts.

Acknowledgments

The authors gratefully acknowledge support from Miami University through the Faculty Research Grants program. The authors also gratefully acknowledge the involvement of others on this project, especially Christian Petty, Catherine Puleo, and Jeffrey Phillip at Miami University for their help and assistance during the early stages of this project.

References

[1] D.L. O'Neal, D.R. Tree, Measurement of frost growth and density in a parallel plate geometry, ASHRAE Trans. 90 (2A) (1984) 278–290.
[2] M.M. Padki, S.A. Sherif, R.M. Nelson, A simple method for modeling the frost formation phenomenon in different geometries, ASHRAE Trans. 95 (2) (1989) 1127–1137.
[3] R. Östin, S. Andersson, Frost growth parameters in a forced air stream, Int. J. Heat Mass Transfer 34 (1991) 1009–1017.
[4] R.W. Rite, R.R. Crawford, A parametric study of the factors governing the rate of frost accumulation on domestic refrigerator-freezer finned-tube evaporator coils, ASHRAE Trans. 97 (2) (1991) 438–445.
[5] T. Senshu, H. Yasuda, K. Oguni, K. Ishibani, Heat pump performance under frosting conditions: Part I – heat and mass transfer on cross-finned tube heat exchangers under frosting conditions, ASHRAE Trans. 96 (1) (1990).
[6] Y. Hayashi, A. Auki, S. Adachi, K. Hori, Study of frost properties correlating with frost formation types, J. Heat Transfer 99 (1977) 239–245.
[7] P.L.T. Brian, R.C. Reid, Y.T. Shah, Frost deposition on cold surfaces, Ind. Eng. Chem. Fund. 9 (3) (1970) 375–380.
[8] D.K. Yang, K.S. Lee, Dimensionless correlations of frost properties on a cold plate, Int. J. Refrig. 27 (2004) 89–96.
[9] D.K. Yang, D.H. Lee, J.S. Kim, K.S. Lee, Modeling of frost behavior on a cold plate, in: Proc. of the Int'l Refrig. and Air Conditioning Conference at Purdue, West Lafayette, IN, July 12–15, Paper No. R121, 2004.
[10] J.D. Yonko, S.F. Sepsy, An investigation of the thermal conductivity of frost while forming on a flat horizontal plate, ASHRAE Trans. 73 (2) (1967) 1.1–1.11.
[11] K.S. Lee, W.S. Kim, T.H. Lee, A one-dimensional model for frost formation on a cold flat surface, Int. J. Heat Mass Transfer 40 (18) (1997) 4359–4365.
[12] C.-H. Cheng, Y.-C. Cheng, Predictions of frost growth on a cold plate in atmospheric air, Int. Commun. Heat Mass Transfer 28 (7) (2001) 953–962.
[13] B.W. Jones, J.D. Parker, Frost formation with varying environmental parameters, J. Heat Transfer 97 (1975) 255–257.
[14] S.A. Sherif, S.P. Raju, M.M. Padki, A.B. Chan, A semi-empirical transient method for modeling frost formation on a flat plate, Int. J. Refrig. 16 (5) (1993) 321–329.
[15] C.-H. Cheng, K.-H. Wu, Observations of early-stage frost formation on a cold plate in atmospheric air flow, J. Heat Transfer 125 (2003) 95–102.
[16] B. Na, R.L. Webb, New model for frost growth rate, Int. J. Heat Mass Transfer 47 (2004) 925–936.
[17] B. Na, R.L. Webb, Mass transfer on and within a frost layer, Int. J. Heat Mass Transfer 47 (2004) 899–911.
[18] H.W. Schneider, Equation of the growth rate of frost forming on cooled surfaces, Int. J. Heat Mass Transfer 21 (1978) 1019–1024.
[19] Y.X. Tao, R.W. Besant, K.S. Rezkallah, A mathematical model for predicting the densification and growth of frost on a flat plate, Int. J. Heat Mass Transfer 36 (2) (1993) 353–363.
[20] J.E. White, C.J. Cremers, Prediction of growth parameters of frost deposits in forced convection, J. Heat Transfer 103 (1981) 3–6.
[21] R. Yun, Y. Kim, M. Min, Modeling of frost growth and frost properties with airflow over a flat plate, Int. J. Refrig. 25 (3) (2002) 362–371.
[22] H. Inaba, S. Imai, Study on sublimation phenomenon of horizontal frost layer exposed to forced convection air flow and radiant heat, J. Heat Transfer 118 (1996) 694–701.
[23] R. Le Gall, J.M. Grillot, Modeling of frost growth and densification, Int. J. Heat Mass Transfer 40 (13) (1997) 3177–3187.
[24] K. Ogawa, N. Tanaka, M. Takeshita, Performance improvement of plate fin-and-tube heat exchangers under frosting conditions, ASHRAE Trans. 99 (1) (1993) 762–771.
[25] C.J.L. Hermes, F.R. Loyola, V.S. Nascimento Jr., A semi-empirical correlation for the frost density, Int. J. Refrig. 46 (2014) 100–104.
[26] V.S. Nascimento Jr., F.R. Loyola, C.J.L. Hermes, A study of frost build-up on parallel plate channels, Exp. Therm. Fluid Sci. 60 (2015) 328–336.
[27] J.L. Hoke, J.G. Georgiadis, A.M. Jacobi, Effect of substrate wettability on frost properties, J. Thermophys. Heat Transfer 18 (2) (2004) 228–235.
[28] E.U. Okoroafor, M. Newborough, Minimizing frost growth on cold surfaces exposed to humid air by means of crosslinked hydrophilic polymeric coatings, Appl. Therm. Eng. 20 (2000) 737–758.
[29] J. Shin, A.V. Tikhonov, C. Kim, Experimental study on frost structure on surfaces with different hydrophilicity: density and thermal conductivity, J. Heat Transfer 125 (2003) 84–94.
[30] S.A. Kulinich, S. Farhadi, K. Nose, X.W. Du, Superhydrophobic surfaces: are they really ice-repellent?, Langmuir 27 (1) (2011) 25–29
[31] H. Lee, J. Shin, S. Ha, B. Choi, J. Lee, Frost formation on a plate with different surface hydrophilicity, Int. J. Heat Mass Transfer 47 (2004) 4881–4893.